Spin interaction and magnetism in cobaltate Kitaev candidate materials: An *ab initio* and model Hamiltonian approach

Shishir Kumar Pandey and Ji Feng *
International Center for Quantum Materials, School of Physics, Peking University, Beijing 100871, China

(Received 8 May 2022; accepted 1 November 2022; published 14 November 2022)

In the quest for materials hosting Kitaev spin liquids, much of the efforts have been focused on the fourth- and fifth-row transition metal compounds, which are spin-orbit coupling–assisted Mott insulators. Here we study the structural and magnetic properties of 3*d* transition metal oxides, $Na_2Co_2TeO_6$ and $Na_3Co_2SbO_6$. The partial occupancy of sodium in former compound is addressed using a cluster expansion, and a honeycomb lattice of sodiums is found to be energetically favored. Starting from the *ab initio* band structures, a many-body second-order perturbation theory leads to a pseudospin-$\frac{1}{2}$ Hamiltonian with estimated magnetic interactions. We show that the experimentally observed zigzag magnetic state is stabilized only when the first-neighbor Kitaev coupling dominates over the Heisenberg term, both of which are highly suppressed due to presence of e_g orbitals. A third-neighbor Heisenberg interaction is found dominant in both these compounds. We also present a phase diagram for $Na_2Co_2TeO_6$ by varying the electron-electron and spin-orbit interactions. The computed spin excitation spectra are found to capture essential features of recent experimental magnon spectrum, lending support to our results.

DOI: 10.1103/PhysRevB.106.174411

I. INTRODUCTION

Strong quantum fluctuations in the ground state of a many-spin system can produce a quantum spin liquid state, in which spins are highly entangled even at large separations without any long-range order [1,2]. Realization of quantum spin liquid in actual materials is clearly attractive, especially for its potential application in quantum computation [3] and high-T_c superconductivity [4]. Known candidate materials that may host a spin liquid state are few [5–8], and the quest for new potential candidates has recently drawn a lot of attention triggered by the pioneering work of Kitaev who proposed an exactly solvable spin model on triply coordinated lattice, exhibiting degenerate spin-liquid ground states [3]. Extension of the Kitaev's honeycomb lattice model [9] to the inclusion of bond-dependent, highly anisotropic Heisenberg coupling interactions inherently introduces frustration to the spin system and may be conducive to the realization of quantum spin liquid states.

A host of transition-metal compounds have been proposed as a material candidates for realizing the Kitaev physics [10–24]. Nevertheless, compounds containing a 3*d* element distinguishes themselves from 4/5*d* compounds. On the one hand, crystal fields (CF) and spin-orbit coupling (SOC) are believed to be substantially stronger in 4/5*d* compounds than in their third-row counterparts. On the other hand, 3*d* elements are considerably more compact and the localization of *d* orbitals results in larger Hubbard U and intra-atomic Hund's coupling compared to 4/5*d* compounds. Much of previous attention has been paid to 4/5*d* magnetic materials, in which the interplay of Hubbard interaction (U), intra-atomic Hund's exchange (J_H), CF (Δ), and the SOC (λ) leads to intricate Mott insulating states [25–37]. The studies focusing 3*d* material are few and limited mostly to theoretical models [10,11,13]. A quantitative examination based on *ab initio* electronic structure methods of the electronic and magnetic structure of the cobased compounds, $Na_2Co_2TeO_6$ and $Na_3Co_2SbO_6$, is evidently in order.

Each Co^{+2} with seven d electrons in a nearly octahedral CF of oxygens in these materials shows a high-spin $t_{2g}^5 e_g^2$ configuration. The d electrons on an isolated Co ion is then described by an effective spin $S = 3/2$ and orbital angular momentum $L = 1$, giving rise to a low-energy pseudospin-1/2 doublet after application of SOC. Similarly to iridates and α-$RuCl_3$, experiments propose zigzag magnetic ground state also for $Na_2Co_2TeO_6$ and $Na_3Co_2SbO_6$ [38–40]. What makes these d^7 cobaltates even more intriguing, compared to those of d^5 iridates or α-$RuCl_3$, is the additional presence of spin-only active e_g orbitals.

In transition metal compounds, the origin of anisotropic magnetic interactions such as Kitaev interaction is attributed to a combination of the directional nature of transition metal d orbitals and the interaction of unquenched orbital moments with spin moments via spin-orbit interaction (SOI), which may give rise to this type of nontrivial anisotropic exchange coupling. Under the large CF present in these 4/5*d* compounds, the low-energy excitations of d^5 configuration of transition metal ions can be described by a single hole with an effective spin moment $S = 1/2$ and an effective orbital angular moment $L = 1$ within the t_{2g} manifold. The SOI then leads to an effective total angular momentum of $J_{\text{eff}} = S - L$, forming for a pseudospin-1/2 corresponding to doubly degenerate ground state.

Based on the above discussions, several interesting questions arises about structural, electronic, and magnetic properties of cobaltates. Whether cobaltates are a Kitaev-type material, and if so, how close it is to a quantum spin liquid,

*jfeng11@pku.edu.cn

are questions worth pursuing. Additionally, whether the small structural difference in the two compunds, explained later, can bring some noticable changes in the magnetic interactions would be a crucial information from an experimental perspective. Pertaining to the structure-property relation, how the Na partial occupancy in $Na_2Co_2TeO_6$ impacts its electronic or the magnetic properties clearly requires investigation.

In the present study, the fractional occupancy of Na in $Na_2Co_2TeO_6$ is first resolved computationally using the cluster expansion technique, with which we obtain particular pattern formation of Na atoms in the supercell of $Na_2Co_2TeO_6$. Subsquently, the magnetic interactions between the Co^{+2} ions in terms of pseudospins-1/2 for both $Na_2Co_2TeO_6$ and $Na_3Co_2SbO_6$ are obtained based on the second-order perturbation theory. The hopping amplitudes and CF splitting considered in this method are estimated from tight-binding (TB) models obtained from fitting the *ab initio* electronic structures. We show that Heisenberg interactions as well as off-diagonal couplings are all highly suppressed and the dominant interaction is Kitaev type for first-nearest-neighbor (1NN) Co atoms. Trigonal CF splitting, albeit comparable to the strength of SOC in these materials, does not alter the pseudospin-1/2 picture. The second-nearest-neighbor (2NN) and interlayer magnetic interactions are found to be negligibly small. Contrary to $4d/5d$-based Kitaev materials, quite surprisingly, the third-nearest-neighbor (3NN) magnetic interactions are significantly larger than the 1NN ones. Remarkably, a suppressed Kitaev coupling and appearance of off-diagonal terms are revealed for 3NNs. The spin-wave spectra obtained using these magnetic interactions in a Heisenberg-Kitaev model shows qualitative agreement with experiments. By varying parameters Hubbard U and SOC strength-λ we obtain a phase diagram for $Na_2Co_2TeO_6$. We find different type of zigzag magnetic ordering stabilized in major portion of the phase diagram. We extensively discuss the properties of $Na_2Co_2TeO_6$ in this study and finish our discussion in the end with a brief comparison between the properties of $Na_2Co_2TeO_6$ and $Na_3Co_2SbO_6$.

II. METHODS

Before proceeding to the discussions of the crystal and basic electronic structures, let us briefly describe the computational details of the *ab initio* calculations for basic electronic structure and total energies and of the cluster expansion and Monte Carlo simulation employed to understand the Na vacancy in $Na_2Co_2TeO_6$.

A. *Ab initio* and TB calculations

To calculate the total energies and electronic structure of cobaltates, we perform density-functional theory (DFT) calculations with the generalized-gradient approximation (GGA) within Perdew-Burke-Ernzerhof framework [41]. Calculations were performed using Vienna *ab initio* simulation package (VASP, version-5.4.4) [42]. Plane-wave basis set with a cutoff at 550 eV with projected augmented wave potentials [43,44] is used, with a $8 \times 8 \times 4/6 \times 3 \times 6$ $\boldsymbol{k}$-grid for the Brillouin zone sum for calculations on the primitive cell of $Na_2Co_2TeO_6/Na_3Co_2SbO_6$, and a $6 \times 6 \times 3$ $\boldsymbol{k}$-grid for the supercell to be described later. To account for the correlation in Co(II) d states, a static on-site U is used in the GGA + U formalism [45]. SOI was included along with spinor wave functions in the nonrelativistic approximation. The total energies are calculated self-consistently till the energy difference between successive steps was better than 0.5^{-6} eV/formula unit. All results are sufficiently converged for this choice of basic computational parameters. Using Na vacancy configuration obtained from our cluster expansion calculations (discussed next) along with the experimentally observed zigzag magnetic ground state, a full structural optimization relaxing both ion positions and lattice parameters using $U = 3$ eV leads to lattice parameters within 1.4% of the experimental values. We hence use the experimental crystal structures in all subsequent *ab initio* band structure calculations.

To extract the CF matrix and hopping matrix elements, a TB Hamiltonian describing the low-energy states of both the materials were constructed using the maximally localized Wannier function implemented in Wannier90 package [46]. We consider all the five Co d orbitals in the TB basis. The strength of SOI $\lambda = 65$ meV is determined by fitting the SOC included *ab initio* band structure with the TB model after explicitly introducing the intratomic SOC term ($\sum_i \lambda \boldsymbol{L}_i \cdot \boldsymbol{s}_i$ where i is site index) in the model. The band structure fit is shown in Fig. 3(b).

B. Cluster expansion and Monte Carlo simulations

The issue of Na partial occupancy in $Na_2Co_2TeO_6$ is resolved using a cluster-expansion model to aid a global survey of the energy landscape of the vacancy disorder. The total energy of $Na_2Co_2TeO_6$ with 2/3 Na occupancy in $Na_2Co_2TeO_6$ is expressed as a cluster expansion up to the fourth order, as

$$E(\mathcal{C}) = E_0 + \sum_{\alpha} g_\alpha V_\alpha \varphi_\alpha, \tag{1}$$

where a configuration $\mathcal{C}$ refers to particular occupation of the lattice conforming to 2/3 occupancy of a Na monolayer, V_α are the effective cluster interactions associated with the symmetry inequivalent cluster α with multiplicity g_α, and φ_α are the cluster correlations calculated as symmetrized averages of the products of all lattice sites (1, 2, 3, and 4 for one-, two-, three-, and four-point clusters) over the number of unit cells needed to form the cluster α in configuration $\{\mathcal{C}\}$. Cluster spaces with up to four-point clusters (quadruplets) comprised of 132 distinct clusters are considered. Further improvement on the model is not seen on inclusion of higher-order clusters. The effective cluster interactions V_α are obtained using least absolute shrinkage and selection operator as implemented in the ICET package [47]. The total energies of a $2 \times 2 \times 1$ supercell obtained from *ab initio* calculations are used to train and cross-validate the model in Eq. (1). The model is subsequently employed in Monte Carlo simulations in the canonical ensemble to obtain the lowest-energy configuration with Na vacancies. The Monte Carlo annealing processes start from a sufficiently high temperature of 1000 K, to avoid trapping into local minima. The annealing proceeds by lowering the temperature as a function of Monte Carlo steps with function T_{start} - (T_{start} - T_{stop}) × log(step + 1)/log(n_{steps}) where T_{start}

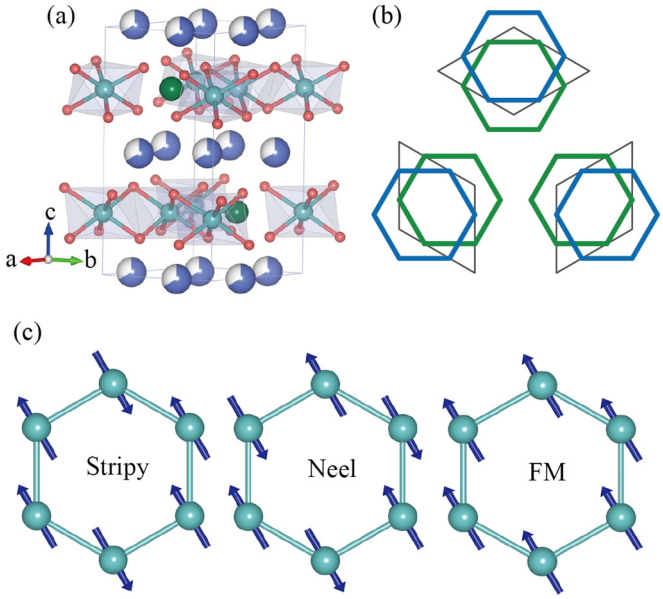

FIG. 1. Crystal and magnetic structures of $Na_2Co_2TeO_6$. (a) Crystal structure. Cyan, red, and green balls represent Co, O, and Te, respectively. Blue-white balls represent 2/3 partial occupancy of Na atoms in $Na_2Co_2TeO_6$. (b) Top view of the lowest-energy Na network in two layers of $Na_2Co_2TeO_6$ unit cell obtained in our cluster expansion model, in accordance with an average 2/3 occupancy of the Na sites. Each of the layer forms a honeycomb lattice, shown as blue and green hexagons, respectively. The stacking of the bilayer breaks C_3 symmetry, as is evidenced by inspecting the three C_3 related replicas. (c) Possible magnetic structures in a single-layer honeycomb lattice of Co atoms, showing the stripy, Néel, and ferromagnetic configurations.

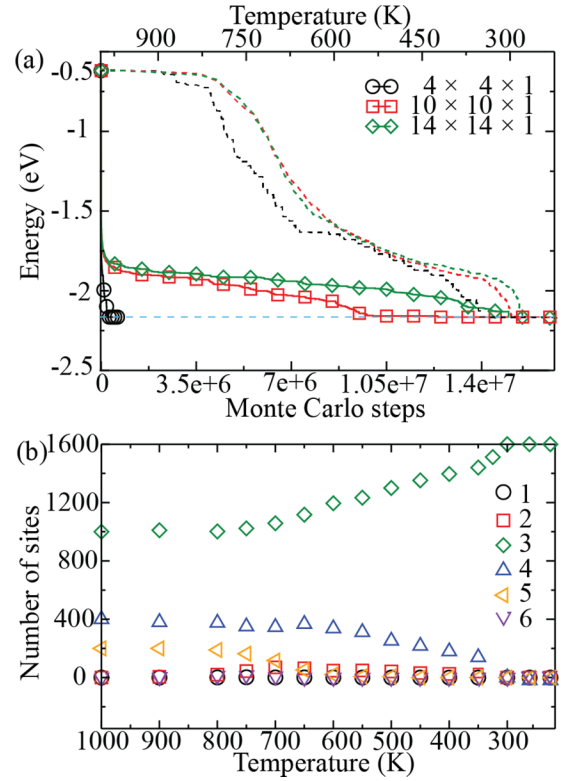

FIG. 2. (a) Variation in configurational energy per atom with temperature (top three dashed lines) and with Monte Carlo steps (lower three solid lines) obtained in annealing process for various supercells. Horizontal dashed line represents the ground-state energy. Different plateaus of energy in the equilibration process (dashed lines) is clearly visible with the flat plateau in range 300–225 K revealing that ground state has reached. (b) Change in coordination of Na sites with temperature for 10 ×10 × 1 supercell. For ground state, only three-point clusters are present with population of all other clusters vanishing with lowering of temperature.

(T_{stop}) is the starting (target) temperatures, and n_{steps} (step) is the total number of Monte Carlo steps (current step). We obtain the ground state at 300 K in each case which remain so with further lowering of temperature close to zero. We set the lower temperature at 225 K in our Monte Carlo simulations. The Na monolayer $n \times n$ supercells with ($n = 4, 10, 14$) were used in our simulations. Typically, a system is annealed in 2^6–2^8 steps, depending on system size, to avoid mode collapsing. MC simulations were performed using the same ICET package [47].

III. $Na_2Co_2TeO_6$

A. Structure and Na vacancies

In this section, we present the results concerning the basic structure and electronic structure of $Na_2Co_2TeO_6$ obtained from *ab initio* calculations. We will discuss properties of $Na_3Co_2SbO_6$ later in Sec. IV. As shown in Fig. 1(a), in the experimental crystal structure of $Na_2Co_2TeO_6$ [12,14,15,38,38–40] Co(II) ions are caged in edge-sharing oxygen octahedra, forming a honeycomb lattice with a Te ion sitting in the center of each hexagon. These two-dimensional Co-O-Te sheets are joined by hexagonal close-packed Na monolayers to form a three-dimensional array, with hexagonal lattice in the space group $P6_322$. It was found that the intercalated Na layers has a 2/3 overall occupancy, though the sixfold symmetry remains intact. Not only this presents a challenge to DFT calculations, the charge pattern of the partially occupied Na layers can also influence the spin states and interactions which is the central topic of present study. Therefore, we begin by sorting out this issue before performing further analysis of the electronic and spin structures.

To this end, we perform cluster expansion calculations in which random starting vacancy configurations conforming to 2/3 occupancy invariably converge to a honeycomb lattice, when annealed from over 1000 K steadily down to 300 K. The energy evolution for different supercells in the simulated annealing processes is shown in Fig. 2(a), which all evidently converge to the same ground state. We stress that the energy in this plot is the configurational potential energy of Na vacancies, which shows several steps in various temperature ranges before plateauing at 300 K for ground-state configuration. Lowering the temperature further to 225 K does not change the energy, reassuring that the system is well equilibrated. The evolution of coordination numbers of Na for a 10 × 10 supercell during a typical annealing is shown in Fig. 2(b). The population of triply coordinated Na sites increases gradually as the annealing proceeds, while the population of atoms with

TABLE I. Energies of various magnetic configurations (in eV) relative to the zigzag antiferromagnetic configuration.

	Spin direction		
Mag. config.	010	001	100
Zigzag	0.0	0.226	0.231
Stripy	0.338	1.688	0.116
Neel	0.724	0.737	0.758
FM	0.252	0.073	0.086

other coordination numbers diminish. The resultant structure at 300 K only has triply coordinated sites, corresponding to a honeycomb lattice. These results point to the honeycomb net as a most probable ground-state monolayer configuration. However, when we stack two of such these honeycomb lattices together in a given experimental unit cell, where the original hexagonal close-packed sheets adopt a *ABAB* type periodic stacking, it is seen the unit cell cannot have threefold rotational symmetry. As shown in Fig. 1(b), the three replica of such bilayer stacking with a unit cell interrelated by C_3 rotations are shown. Clearly, these replica do not coincide with each other, demonstrating the the lack of threefold symmetry in this *ordered* Na vacancy configuration.

We thus come to the following interpretation of the computed Na vacancy configuration in order to reconcile with the experimentally established crystal structure with an apparent threefold symmetry. Within each layer, the Na vacancies are arranged to produce an ordered honeycomb lattice, and the layer stacking is disordered owning to weak interlayer interactions to produce an overall threefold symmetry in elastic scattering experiments. For example, for an in-plane reciprocal lattice vector $\boldsymbol{g} \cdot \boldsymbol{c} = 0$, the structure factor of the Na sublattice is

$$S(\boldsymbol{g}) = n\,\overline{\exp(-i\boldsymbol{g}\cdot\boldsymbol{d})},$$

where n is the atom number density, $\boldsymbol{d}$ is the location of sodium in a two-dimensional honeycomb sheet within a unit cell, and the overbar means averaging over all layers. Clearly, given the presumed stacking disorder, the three configurations in Fig. 1(b) contribute equally to the average and $S(\boldsymbol{g})$ shall have threefold symmetry.

B. Electronic structure

Therefore, we shall adopt one of the three equivalent Na configurations in Fig. 1(b) in the *ab initio* calculations. Note, however, that the threefold symmetry will be imposed on the TB Hamiltonian based on which magnetic interactions are extracted and discussed later.

Once the SOI is included self-consistently in our calculations in the structure described above, the experimentally proposed zigzag antiferromagnetic ground state can be reproduced. The total energy for various magnetic configuration is listed in Table I and shown in Fig. 1(c) [for zigzag configuration, see Fig. 4(b)]. The spin magnetic moments of Co atoms in the ground state were found to be 2.69 μ_B, comparable with the experimentally observed value of 2.77 μ_B and a little smaller than what is expected for an effective 3/2-spin system.

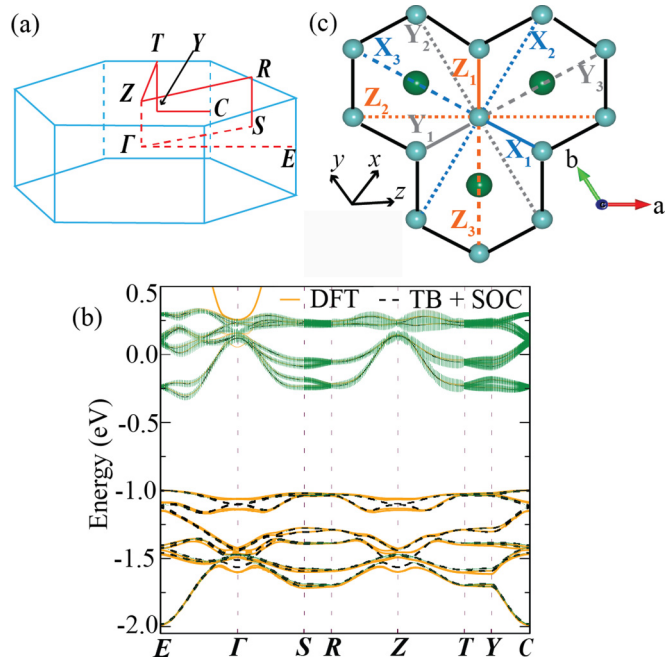

FIG. 3. (a) Brillouin zone of $Na_2Co_2TeO_6$. (b) *Ab initio* band structure with SOC fitted with TB Hamiltonian with SOI. The fat band representation depicted in green shows e_g contribution of Co-*d* orbitals. The Fermi energy is set to zero. (c) A single-layer Co^{+2} lattice in $Na_2Co_2TeO_6$. 1NN, 2NN, and 3NN bonds are indicated by solid, dotted, and dashed lines, respectively. Orange, dark gray, and light blue color represent the Z, Y, and X bonds, respectively. *a*, *b*, and *c* are the crystallographic axes and cubic axes of Co-O octahedra are denoted by *x*, *y*, and *z*.

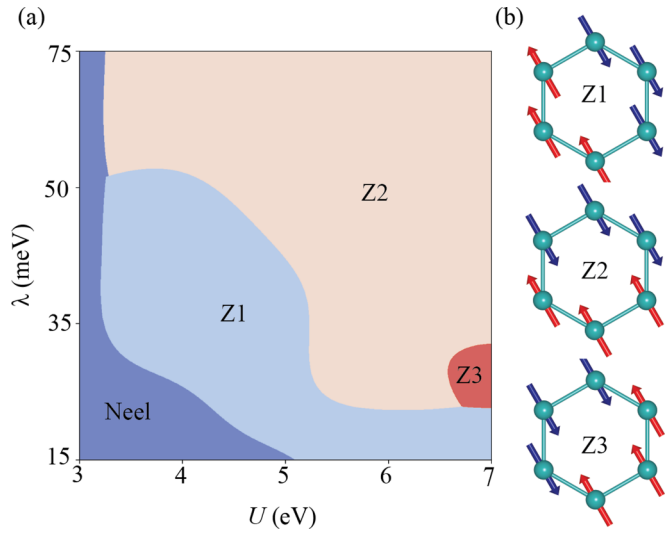

FIG. 4. (a) The U-λ phase diagram for $Na_2Co_2TeO_6$at $J_H/U = 0.16$. Magnetic ground state obtained classically with magnetic interactions extracted in different regions of the phase space brings four distinct phases, a Neel, and three zigzag phases Z1, Z2, Z3 shown in (b). These three zigzag phases differ by the direction of antiferromagnetic coupling between the two ferromagnetic chains in a hexagon. Z1 is the experimentally proposed magnetic state in which antiferromagnetic coupling is along the X bond shown in Fig. 3(c).

In order to extract the magnetic interactions, we construct a TB Hamiltonian as described in the methods section. The crystal structure of cobaltates have a C_3 axis along crystallographic c axis. We choose the local axes x, y, z along Co-O bonds such that $x + y + z = c$, i.e., the local axes commensurate with threefold symmetry of the crystal structure. Mapping in this setting of local axes is done considering a basis formed by all the five d orbitals on Co atoms. The Brillouin zone of $Na_2Co_2TeO_6$ is shown in Fig. 3(a). The *ab initio* band structure for the nonmagnetic phase shown in Fig. 3(b) in a calculation involving SOC shows that the low-energy excitation involves both the e_g and t_{2g} states. Thus the Wannier functions involve the full set of d orbitals on Co. Using the basis $\psi^\dagger_{i\sigma} = [d^\dagger_{z^2}, d^\dagger_{xz}, d^\dagger_{yz}, d^\dagger_{x^2-y^2}, d^\dagger_{xy}]_{i\sigma}$ for site i and spin σ, the TB Hamiltonian then reads

$$\begin{aligned} H_0 &= H_{\rm cf} + H_{\rm hop} + H_{\rm soc} \\ &= \sum_{i,\sigma} \psi^\dagger_{i\sigma} \Delta_i \psi_{i\sigma} + \sum_{i\neq j,\sigma} \psi^\dagger_{i\sigma} T_{ij} \psi_{j\sigma} + \sum_i \lambda \boldsymbol{L}_i \cdot \boldsymbol{s}_i, \quad (2) \end{aligned}$$

in which the CF (Δ_i) and the hopping amplitudes (T_{ij}) are obtained from the TB model without SOI. The so-determined spin-independent CF matrix (in eV) is

$$\Delta_i = \begin{bmatrix} 1.377 & 0.045 & 0.045 & 0.000 & 0.089 \\ 0.045 & 0.015 & 0.006 & 0.078 & -0.006 \\ 0.045 & 0.006 & 0.051 & -0.077 & -0.006 \\ 0.000 & 0.078 & -0.078 & 1.377 & 0.000 \\ 0.089 & -0.006 & -0.006 & 0.000 & 0.015 \end{bmatrix}. \quad (3)$$

This CF matrix has explicit C_3 symmetry. The spin-independent hopping amplitudes are listed in Table IV. These parameters are used in the next set of calculations. The last term in Eq. (2) is the atomic SOI. It is observed that the strength of SOI ($\lambda = 65$ meV, see Methods) in $Na_2Co_2TeO_6$ is considerably smaller than that of Ir- and Ru-based materials, for which $\lambda \approx 400$ meV [48] and 150 meV [18], respectively.

C. Magnetic interaction and magnetism

Before investigating in detail the magnetic properties of $Na_2Co_2TeO_6$, it is important to discuss its structural and electronic features. A comparison between $Na_2Co_2TeO_6$ and previously studied $4/5d$ materials with pseudospin-1/2 ground state highlights the following crucial differences between these materials. Additional presence of e_g orbitals for Co^{+2}-d^7 with active spin only degree of freedom put this material in a different class when compared to the materials with d^5 configuration. Also, magnitude of trigonal CF in $Na_2Co_2TeO_6$ [~ 27 meV, see the matrix in Eq. (3)] is expected to be of the same order as that of the SOC strength (λ) which further distinguishes this material from those of $4d/5d$-based compounds where λ is an order of magnitude larger than the trigonal CF. As λ is responsible for energy separation between $J_{\rm eff}$-1/2 and $J_{\rm eff}$-3/2 states while trigonal CF mixes these states, this separation is expected to be smaller in $Na_2Co_2TeO_6$.

From a structural perspective, Co-O-Co angles across a pair of edge-sharing octahedra are $\sim 92^\circ$ which is close to the ideal case of 90°. In contrast, the same metal-ligand-metal bond angles in Na_2IrO_3 and α-$RuCl_3$ are significantly larger: 100° for the former and 94° for the latter [17,22]. This difference manifests itself in terms of enhanced direct (σ-type) hopping amplitudes between d orbitals of Co atoms [34]. For example, in Table IV, $d_{yz} - d_{yz}$ hopping on a X bond is larger when compared to other hopping interactions. The same is true for $d_{zx} - d_{zx}$ and $d_{xy} - d_{xy}$ hopping on Y and Z bonds. Opposite has been observed in case of Na_2IrO_3 [34].

To be concrete, let us consider the interaction Hamiltonian

$$H_{\rm int} = \frac{U}{2} \sum_{i,\alpha} n_{i\alpha\sigma} n_{i\alpha\sigma'} + \frac{U'}{2} \sum_{i,\alpha\neq\beta} n_{i\alpha} n_{i\beta} - \frac{J_H}{2} \sum_{i,\sigma,\sigma',\alpha\neq\beta} \psi^\dagger_{i\alpha\sigma} \psi_{i\alpha\sigma'} \psi^\dagger_{i\beta\sigma'} \psi_{i\beta\sigma} - \frac{J'}{2} \sum_{i,\sigma\neq\sigma',\alpha\neq\beta} \psi^\dagger_{i\alpha\sigma} \psi_{i\beta\sigma'} \psi^\dagger_{i\alpha\sigma'} \psi_{i\beta\sigma}. \quad (4)$$

Here U/U' are intraorbital/interorbital Hartree energies, and J_H and J' are Hund's coupling and pair hopping interaction, respectively. Rotational invariance in the single-atom limit dictates the relationships: $U' = U$ - $2J_H$ and $J_H = J'$.

The key here is the d^7 manifold has a twofold degenerate ground state, which form a Kramers doublet and can be treated as a pseudospin-1/2. In order to extract the magnetic interactions of these pseudospin states, we first project the full TB Hamiltonian onto the pseudospin $J_{1/2}$ space $\{\phi_{i\alpha}\}$, $\alpha = \uparrow, \downarrow$, where $\uparrow, \downarrow$ refer to the SOC pseudospin-1/2 states. We note here that due to consideration of local axes x, y, and z in the forthcoming calculations, up/down axis of the pseudo-spins are along c axis which is also the trigonal distortion axis of Co-O octahedra in $Na_2Co_2TeO_6$. We start in the isolated atom limit, where $H_{\rm atom} = H_{\rm cf} + H_{\rm soc} + H_{\rm int}$, and introduce the hopping contribution $H_{\rm hop}$ as a perturbation. In the second-order perturbation theory, the Hamiltonian is written as

$$H^{(2)} = \sum_{ij} \sum_{\alpha\beta\alpha'\beta'} \mathcal{H}(i,j)_{\alpha\beta\alpha'\beta'} |i\alpha, j\beta\rangle \langle i\alpha', j\beta'|, \quad (5)$$

$$\mathcal{H}(i,j)_{\alpha\beta\alpha'\beta'} = \sum_{kl} \sum_{\gamma\lambda} \frac{1}{\Delta E} \langle i\alpha, j\beta | H_{\rm hop} | k\gamma, l\lambda \rangle \langle k\gamma, l\lambda | H_{\rm hop} | i\alpha', j\beta' \rangle, \quad (6)$$

where $1/\Delta E = \frac{1}{2}[1/(E_{i\alpha} + E_{j\beta} - E_{k\lambda} - E_{l\gamma}) + 1/(E_{i\alpha'} + E_{j\beta'} - E_{k\lambda} - E_{l\gamma})]$. Here $|i\alpha, j\beta\rangle$ and $|i\alpha', j\beta'\rangle$ are two-site states in the $J_{1/2}$ ground states, and $|k\lambda, l\gamma\rangle$ are two-site excited states, both in the isolated atom limit. $H_{\rm hop}$ connects a two-site ground state to an excited state with (d^6, d^8) configuration, the dimensions of whose Hilbert spaces are 210 and 45, respectively. The eigenstates of isolated Co with 6, 7, and 8 d electrons are obtained by exact diagonalization.

Considering the scenario when magnitude of Hubbard U and CF splitting are much larger than the hopping amplitudes and also when the SOC strength is much larger than t^2/U, the low-energy space is formed by the lowest two degenerate many body states of the "on-site" Hamiltonian (H_{atom}). These states behaves exactly as psuedospin-1/2 Kramers doublet in the limit of an infinite CF and in the absence of any lattice distortions which can further split the t_{2g} orbitals such as trigonal distortions. Writing the pseudospin $J_{1/2}$ as $S^\mu = \frac{1}{2}\sigma^\mu$, Eq. (6) can be mapped to a spin Hamiltonian of the form

$$H_{\text{spin}} = S_i^\mu \Gamma(i,j)^{\mu\nu} S_j^\nu = \tfrac{1}{4}\Gamma(i,j)^{\mu\nu}\phi_{i\alpha}^\dagger \sigma_{\alpha\alpha'}^\mu \phi_{i\alpha'}\phi_{j\beta}\sigma_{\beta\beta'}^\nu \phi_{j\beta}^\dagger, \tag{7}$$

where $\mu, \nu = 0, x, y, z$, σ^μ are Pauli matrices, and summation over all repeated indexes is implied. The map can be achieved by solving the linear equations

$$-\tfrac{1}{4}\sigma_{\alpha\alpha'}^\mu \sigma_{\beta\beta'}^\nu \Gamma(ij)^{\mu\nu} = \mathcal{H}(i,j)_{\alpha\beta\alpha'\beta'}. \tag{8}$$

The spin Hamiltonian thus can be rewritten as

$$\begin{aligned} H_{\text{spin}} = &\sum_{\langle i,j\rangle \in l(mn)} \left[J_1^l \boldsymbol{\sigma}_i \cdot \boldsymbol{\sigma}_j + K_1^l \sigma_i^l \sigma_j^l + \eta_1^l \left(\sigma_i^m \sigma_j^n + \sigma_i^n \sigma_j^m\right) + \eta_1'^l \left(\sigma_i^m \sigma_j^l + \sigma_i^n \sigma_j^l + \sigma_i^l \sigma_j^m + \sigma_i^l \sigma_j^n\right)\right] \\ &+ \sum_{\langle\langle\langle i,j\rangle\rangle\rangle \in l(mn)} \left[J_3^l \boldsymbol{\sigma}_i \cdot \boldsymbol{\sigma}_j + K_3^l \sigma_i^l \sigma_j^l + \eta_3^l \left(\sigma_i^m \sigma_j^n + \sigma_i^n \sigma_j^m\right) + \eta_3'^l \left(\sigma_i^m \sigma_j^l + \sigma_i^n \sigma_j^l + \sigma_i^l \sigma_j^m + \sigma_i^l \sigma_j^n\right)\right]. \end{aligned} \tag{9}$$

Above $\langle i,j\rangle/\langle\langle\langle i,j\rangle\rangle\rangle$ represent 1NN/3NN pairs. The 2NN interaction is omitted as they are negligibly small. J, K, and η are, respectively, the Heisenberg, Kitaev, and off-diagonal interactions on any $l \in$ Z/X/Y bond. For example, for Z-type bond, (mn) is (xy), and so on.

We now comment briefly on the results obtained from diagonalization of the "on-site" Hamiltonian, $H_{\text{atom}} = H_{\text{cf}} + H_{\text{soc}} + H_U$, before going into a detailed discussion of the magnetic interactions in $Na_2Co_2TeO_6$.

1. On-site Hamiltonian: H_{atom}

There are four parameters in H_{atom} viz, U, J_H, λ, and Δ. From the optical spectra on CoO [49], estimated value of Hund's splitting (J_H) is $\sim$0.8 eV. J_H/U ratio in cobaltates is believed to be < 0.2 [10], hence $U = 5$ eV was initially fixed in our calculation of magnetic interactions. $\lambda = 65$ meV obtained from band structure fitting is slightly larger than an estimated value of $\sim$0.015 eV (corresponding to J_{eff}-1/2 to J_{eff}-3/2 transition) from inelastic neutron scattering experiment [12]. Later, we will vary both U and λ to examine their effect on the magnetic interactions. Δ obtained from the atomic Hamiltonian of the TB model is consistent with what is expected for such materials [10,13].

The energy separation between J_{eff}-1/2 and J_{eff}-3/2 states, obtained after diagonalizing H_{atom} with above mentioned parameter values, is $\sim$24 meV which is in close agreement with the experimentally observed value of $\sim$21 meV in $Na_2Co_2TeO_6$ [12] and is much smaller than the expected value of $\sim$100 meV corresponding to $\frac{3}{2}\lambda$ (for $\lambda = 0.065$ eV). We attribute this difference to be arising from large mixing between t_{2g}-e_g orbitals through the trigonal distortions present in $Na_2Co_2TeO_6$. Compression of Co-O octahedra along c axis causes large deviation of O-Co-O angles from the ideal 90° with the smallest and largest angles being $\sim$78° and 97°, respectively. This nonorthogonal local environment causes mixing between different d orbitals. It is worth mentioning here that estimate of λ from experiments would yield a value of 15 meV and yet we obtained $J_{\text{eff}} = 1/2$–$3/2$ separation consistent with experimentally observed value using $\lambda = 65$ meV. This calls for scrupulous attention while estimating λ in the systems with active e_g orbitals and large trigonal distortions. The J_{eff}-3/2 states were found to split into two doublets with an energy separation of $\sim$7 meV. To examine the effect of "imperfect" CF due to additional trigonal distortions, we compare the result to a perfect octahedral geometry with $\Delta = 1.36$ eV. In this case, J_{eff}-1/2 and J_{eff}-3/2 separation increased to 34 meV while the J_{eff}-3/2 states regained their fourfold degeneracy. Although the CF heavily mixes $J_{\text{eff}} = 1/2$–3/2 states, pseudospin-1/2 picture is still relevant in $Na_2Co_2TeO_6$ as both, the U and CF splitting $\Delta_{t_{2g}-e_g}$ are much larger than the hopping amplitudes (t) and $\lambda \gg t^2/U$ still holds in our case.

2. Magnetic interactions

The magnetic interaction on X/Y/Z bonds [see Fig. 3(c)], estimated from the process described above, are tabulated in Table II. Owing to the local site symmetry C_3, we have identical magnetic interactions on all the three bonds. Indeed, the 1NN Heisenberg term is highly suppressed and antiferromagnetic as was expected in this case due to opposite sign of e_g-e_g and t_{2g}-e_g exchange process [10,13]. However, contrary to the previous speculations, the ferromagnetic Kitaev term is also small and found to be an order of magnitude smaller when compared with recent experimental estimation from the fitting of spin-wave dispersion data [12]. The same is true for a comparison with Ru- [36] and Ir- [35] based compounds.

TABLE II. Estimated 1NN and 3NN Heisenberg J, Kitaev K, and off-diagonal η, η' terms in $Na_2Co_2TeO_6$ given in meV. The 2NN interactions as well as terms other than J and K for 1NN were found to be negligibly small. Parameters used are $U = 5$ eV, $J_H = 0.8$ eV, and $\lambda = 65$ meV.

	1NN			3NN		
Bond type	J	K	η/η'	J	K	η/η'
X/Y/Z	0.261	−0.678	0.0	3.153	−0.04	|0.76|

There can be mainly two reasons behind such a reduction. First, smaller hopping amplitudes and large U in our case when compared to $4d/5d$ materials can contribute to this huge reduction. The effect of the latter is verified by reducing U to 2.5 eV while keeping the J_H/U ratio fix at 0.16, in which case the magnitude of both J_1 and K_1 are substantially enhanced, to 1.93 and -1.616 meV, respectively. The other factor contributing to the reduction is the weaker SOI in $Na_2Co_2TeO_6$. We will examine the effect of varying λ in a later section to understand how it affects the magnetic interactions.

Interestingly, all other first-neighbor off-diagonal spin interactions η_1 and η_1' are found to be negligibly small for this particular set of parameters, in contrast to what was obtained for Ir- [35] and Ru-based [36] compounds. Previous arguments for the suppression of the Heisenberg interaction in this material also apply to these off-diagonal interactions. We find the second-neighbor as well as interlayer coupling to be negligibly small, ruling out the possibility of any interlayer interactions and effect of Na vacancies separating these Co hexagons in c direction. This again is in complete agreement with the some experimental observations of negligible interlayer spin interactions [15,40]. The limited magnetic correlations between Co honeycomb layers along c axis observed in the experiments on $Na_2Co_2TeO_6$ was attributed to disordered distribution of Na^+ ions which disrupts any out-of-plane magnetic coupling making it essentially intralayer. Not to a complete surprise, the 3NN in $Na_2Co_2TeO_6$ are also nonzero, similarly to the cases of iridates and α-$RuCl_3$ [35,36].

Surprisingly, however, antiferromagnetic J_3 is larger in magnitude than K_1, and hence is the dominant interaction in $Na_2Co_2TeO_6$. At first glance, it seems unusual given that $3d$ orbitals are more compact compared to their $4d/5d$ counterparts. In $Na_2Co_2TeO_6$, the 3NN hopping can be mediated via Te ions sitting at the center of a Co hexagon. Orbital projected density of states for Te-s/p orbitals (not shown) precludes any significant contribution near the Fermi level where Co-d and O-p have their main contributions. This rules out any direct interaction between Co-d and Te-s/p orbitals. A second possibility for the 3NN interaction is through shared O-p orbitals between these ions, which is favored by the highly suppressed 3NN Kitaev interaction due to a cancellation of anistropic interactions from multiple long-distance pathways. This then allows J_3 to become the largest magnetic interaction in this compound. Off-diagonal couplings of a smaller magnitude appears on these bonds. On a Z bond, η_3 is found to be antiferromagnetic, while η_3' ferromagnetic. However, on X bond or Y bond, signs of these couplings do not follow a specific pattern. On these two bonds, η_3' never becomes ferromagnetic while η_3 can be either ferro- or antiferromagnetic.

In order to examine whether the obtained parameters can reproduce the magnetic ground state of $Na_2Co_2TeO_6$, we optimize the magnetic structure using Hamiltonian of Eq. (9) with spins allowed to rotate in the a-b plane. We find that the classical ground state was zigzag type with the ferromagnetic chains running along a direction coupled antiferromagnetically in direction perpendicular to a [see Fig. 4(b)] with propagation vector $\sim$(0.0, 0.5, 0.0). We call it Z2 structure. This structure is different than the experimentally proposed magnetic structure with propagation vector (0.5, 0.0, 0.0) which we call Z1. However, in the next section we show that one can also obtain Z1 as the classical ground by tuning the parameters of perturbation theory.

3. Phase diagram

We varied U and SOC strength (λ) to study their effect on magnetic interactions and on the ground state. A phase diagram, obtained from optimization of classical ground with magnetic interactions obtained at different U-λ values, is shown in Fig. 4(a). J_H/U ratio has been kept fixed at 0.16 in all these calculations. We obtain four distinct phases, viz., Neel and three types of zigzag magnetic order [Fig. 4(b)] differentiated by direction of antiferromagnetic coupling between the ferromagnetic chains. The phase diagram can be read in the following manner.

In a smaller U range (close to 3 eV), classical magnetic ground state is Neel type and independent of λ. In this region, antiferromagnetic J_1 is dominant over other types of first-neighbor interactions. All these interactions increases with increase in λ with K_1 more rapidly than J_1. At a particular λ, with the increase in U, we find decreasing J_1 and K_1 with J_1 decreasing more rapidly than K_1. After critical values of U and λ, situated on the phase boundary of Neel-Z1/Z2 phase, K_1 term stars to the compete with J_1. Only when $K_1 \geqslant J_1$, the magnetic ground state changes from Neel to one of the zigzag types. Z1 configuration [Fig. 4(b)] with propagation vector $\sim$(0.5, 0.0, 0.0) is the experimentally observed magnetic state of $Na_2Co_2TeO_6$. In Z3 configuration with propagation vector $\sim$(0.5, 0.5, 0.0), antiferromagnetic coupling between ferromagnetic zigzag layers is along (1 1 0) direction. At some of the phase points, spin moments of our classical ground state was found to slightly deviate from b direction owing to small η/η' terms.

Here a couple of remarks are in order. First, neither J_1, K_1 terms nor J_3, η_3/η_3' terms alone can produce the zigzag ground state of $Na_2Co_2TeO_6$ which is a collective efforts of all these terms. Second, these three zigzag spin configurations are distinct and hence break the threefold rotational symmetry. To verify this point we compared the energies of these three configurations at same phase point, $U = 4$ eV and $\lambda = 0.60$ eV, the phase boundary point between Z1 and Z2 configurations. At this point, the obtained magnetic ground state was Z1 type and energies of Z2 and Z3 configurations were higher in energy by 0.010 and 0.015 meV per spin. These differences, when compared with the scale of magnetic coupling strengths, are significant and hence establish the fact of these three zigzag magnetic configurations being distinct. Our three zigzag configurations differ from those proposed in Chen *et al.* [15] as in the latter, the three domains of zigzag configurations are related by threefold rotational symmetry. For further validation of our obtained magnetic interactions, spin-wave spectra are computed and analyzed next.

D. Spin-wave spectra

Recently, several inelastic neutron scattering experiments on $Na_2Co_2TeO_6$ have reported spin-wave spectra of this material [12,15]. A main feature of these reported spectra is gapped dispersive modes with lowest dispersive branch of width around 3 meV and some flat modes around 4.5 and 7 meV.

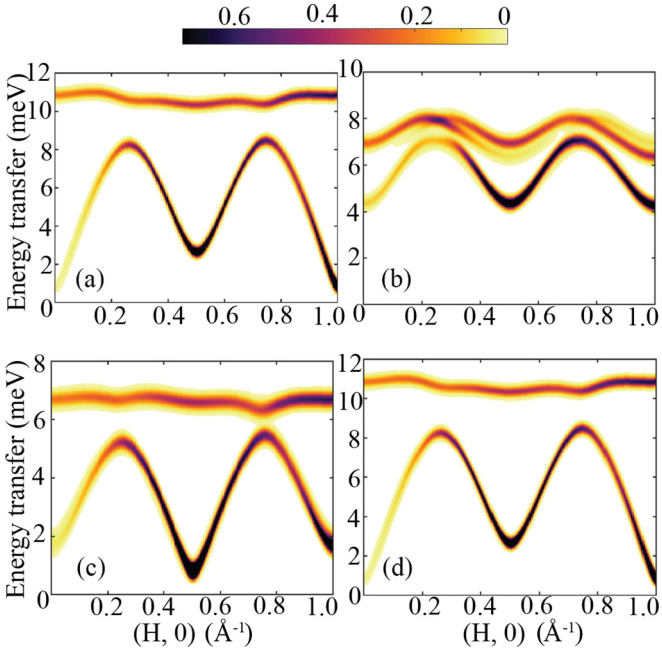

FIG. 5. Spin-wave spectra obtained from linear spin-wave theory for the four phases shown in Fig. 4(a), namely (a) Neel at $U = 3.25$ eV, $\lambda = 0.065$ eV; (b) Z1 at $U = 4$ eV, $\lambda = 0.06$ eV; (c) Z2 at $U = 5$ eV, $\lambda = 0.065$ eV; and (d) Z3 at $U = 7$ eV, $\lambda = 0.025$ eV.

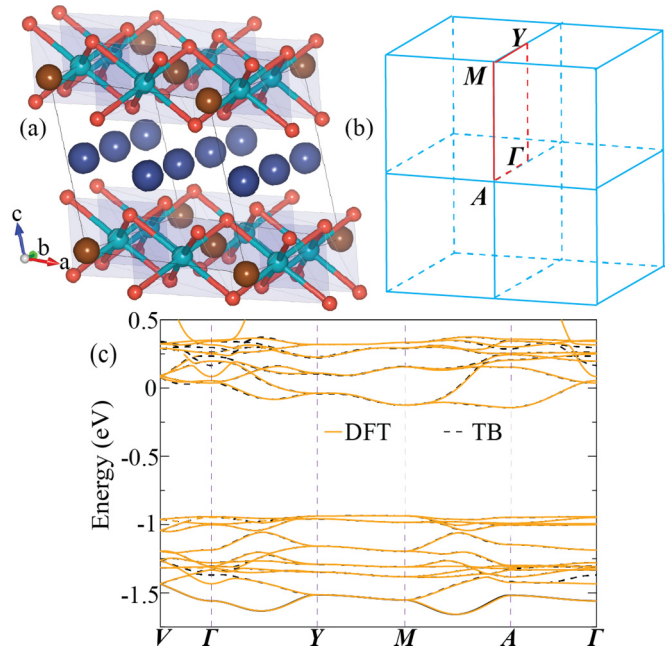

FIG. 6. (a) Crystal structure of $Na_3Co_2SbO_6$. Cyan, red, blue, and brown spheres represent Co, O, Na, and Sb atoms, respectively. Separation of the Co-Sb planes along the c axis by the Na layer is evident and edge-shared Co-O octahedron is also shown. (b) The Brillouin zone of $Na_3Co_2SbO_6$, with some of the high-symmetry points and paths. (c) TB band structure obtained by Wannierizing the *ab initio* electronic structure of $Na_3Co_2SbO_6$ considering all five Co-d orbitals in the basis. Fermi energy is set to zero.

A natural question about how well our estimated magnetic interactions can reproduce these experimental findings is inevitable. The spin Hamiltonian in Eq. (9) with estimated magnetic interactions is solved using the linear spin-wave theory to obtain the spin-wave spectra as implemented in the SpinW package [50]. These calculations are performed for the four distinct magnetic phases in Fig. 4(a) and are shown in Fig. 5.

The spectra of Néel, Z1, and Z3 states are found to differ from the experimentally obtained ones. First, dispersion width of the lowest branch in the spectra of the Néel and Z3 phases [Figs. 5(a) and 5(d)] is much larger (~ 8 meV) than the experimentally observed ~ 3 meV. Though this experimental feature of the spectra is captured in the case of Z1 phase [Fig. 5(b)], a gap of ~ 1 meV with next higher dispersive mode observed in the experiments is missing in this case. Also, this gap is much larger (more than 2 meV) in our calculated spectra for the Neel and Z3 phases. Therefore, our calculated spin-wave spectra for the Z2 phase shown in Fig. 5(c) closely resembles the experimental ones. Though the band width of lowest branch is slightly higher (~ 5 meV) in our model, the computed spectra shown in (c) closely resemble the experimentally observed ones with an M-shaped lowest branch from Chen *et al.* [15] and the higher flat branch with a gap of 1 meV from Songvilay *et al.* [12]. Our calculated spectra also reproduce the gap of ~ 1 meV with next higher branch, consistent with experimental findings [12].

IV. $Na_3Co_2SbO_6$

The crystal of $Na_3Co_2SbO_6$ is shown Fig. 6(a). As for $Na_3Co_2SbO_6$, Co-O-Sb environment is similar to that of Co-O-Te in $Na_2Co_2TeO_6$, except that the two-dimensional sheets of Co-O-Sb are joined by a triangular lattice of Na atoms stacking into the three-dimensional lattice along c direction with space group $C2/m$. Thus, similarly to $Na_2Co_2TeO_6$, the magnetic lattice comprising a Co-honeycomb network in $Na_3Co_2SbO_6$ is quasi-two-dimensional and the magnetic ground state is again a zigzag-type antiferromagnet described by a propagation vector (1/2, 1/2, 0) with the spins aligned along the crystallographic b axis. However, Co-Co distances in $Na_3Co_2SbO_6$ are 10% shorter than $Na_2Co_2TeO_6$. It would hence be interesting to investigate whether such differences in structural features can affect magnetic interactions in $Na_3Co_2SbO_6$. The Brillouin zone of $Na_3Co_2SbO_6$ is shown in Fig. 6(b). Following similar computational procedures to that of $Na_2Co_2TeO_6$, we extracted the CF matrix and hopping interactions for $Na_3Co_2SbO_6$ and fitting of *ab initio* band structure to a Wannier TB model is shown in Fig. 6(c).

The obtained CF matrix and hopping amplitudes are given in Eq. (10) and Table V. Inspection of O-Co-O angles in an octahedra reveal a deviation from the ideal case of 90° to the largest angle being $\sim 96°$ and smallest one being $\sim 81°$. Thus, the lower symmetry of $C2/m$ space group along with the trigonal CF causes the additional splitting of 15 meV within e_g orbitals and two types of splitting 6 and 12 meV within the t_{2g} orbitals. This is consistent with the previous findings on iridates [35] and α-$RuCl_3$ [36]. Co-O-Co angles across a pair of edge-sharing octahedra are $\sim 93.5°$, again close to 90° but slightly larger than the case of $Na_2Co_2TeO_6$. In our

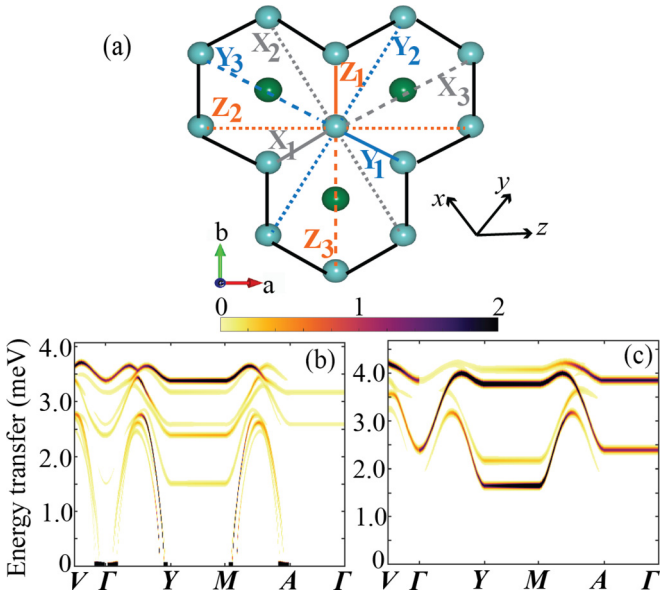

FIG. 7. (a) Lattice of Co^{+2} in $Na_3Co_2SbO_6$. 1NN, 2NN, and 3NN are shown by solid, dotted, and dashed lines. Orange, dark gray, and light blue represent the Z, X, and Y bonds, respectively. a, b, and c are the crystallographic axes and the cubic axes of the Co-O octahedra are denoted by x, y, and z. (b) Spin-wave spectra obtained from linear spin-wave theory for optimized classical ground state of $Na_3Co_2SbO_6$ (at $U = 5.0$ eV, $\lambda = 0.065$ eV) for the case when only in-plane movements of spins were allowed during the optimization. (c) Spectra obtained after full classical optimization of magnetic ground state for which a large out-of-plane deviation of magnetic moments is observed while zigzag configuration remains the ground state.

"on-site" Hamiltonian for $Na_3Co_2SbO_6$, U and λ were kept the same to 5 eV and 65 meV as before. Similarly to the case of $Na_2Co_2TeO_6$, in this case, too, the lowest six states are three Kramer's doublets with energy separation of 28 and ~ 13 meV, between the lowest and the higher two doublets, respectively,

$$\Delta_i = \begin{bmatrix} 1.344 & 0.133 & -0.035 & 0.002 & -0.084 \\ 0.133 & 0.046 & 0.007 & -0.180 & 0.020 \\ -0.035 & 0.007 & 0.016 & -0.093 & 0.022 \\ 0.002 & -0.180 & -0.093 & 1.309 & -0.224 \\ -0.084 & 0.020 & 0.022 & -0.224 & 0.045 \end{bmatrix} \quad (10)$$

For the lower symmetry space group of $Na_3Co_2SbO_6$, symmetry-inequivalent nearest-neighbor bonds have two types, viz-à-viz, Z_1 bonds $\parallel$ to crystallographic b axis with a local C_{2h} point group symmetry and X_1/Y_1 bonds lying in the ab plane with a (lower) C_i point group symmetry. This arrangement of bonds is shown in Fig. 7(a). In such a case, on these X/Y type bonds, in addition to J, K, Γ, and Γ', one needs additional parameters ζ and ξ as explained in Winter *et al.* [35] to describe the magnetic interactions. The magnetic interactions estimated in this case using the second-order perturbation theory is listed in Table III.

By comparing with $Na_2Co_2TeO_6$, we find that the 1NN magnetic interactions are more or less similar in this case.

TABLE III. Estimated 1NN and 3NN Heisenberg J, Kitaev K, and off-diagonal η, η' terms with additional parameters ξ and ζ in $Na_3Co_2SbO_6$ given in meV. The 2NN interactions were found to be negligibly small. Parameters used are $U = 5$ eV, $J_H = 0.8$ eV, and $\lambda = 65$ meV.

Bond type	J	K	η	η'	ξ	ζ
Z_1	0.3	−0.757	0.0	0.0	0.0	0.0
X_1/Y_1	0.186	−0.211	0.0	−0.15	−0.421	0.0
Z_3	1.7	0.4	0.34	−0.31	0.0	0.0
X_3/Y_3	1.823	−0.189	0.31	0.0	−0.211	0.302

However, a subtle difference can be found for the 3NN interactions as in $Na_3Co_2SbO_6$, the magnitudes are half of their values of $Na_2Co_2TeO_6$. Another difference between these two materials is that the Kitaev coupling on Z_3 bond, though again smaller, is found to be antiferromagnetic in this case. Additionally, the η_3/η'_3 terms are much smaller (almost half) in this case when compared to $Na_2Co_2TeO_6$.

With these magnetic parameters in optimization of classical ground state using the Hamiltonian in Eq. (9), only in-plane movement of spins is allowed first which brings the same zigzag type magnetic ground which was obtained experimentally. However, we find a small deviation of spin from b direction along the a axis in our optimized structure in this case, too. In terms of the propagation vector, the optimized magnetic structure is described by $\sim(0.498, 0.492, 0)$. Using this optimized magnetic structure we calculate the spin-wave spectra of $Na_3Co_2SbO_6$ shown in Fig. 7(b). Most of the intensity of this spectra is found in the 3 to 4 meV energy range, which is in reasonably good agreement with the recent experiment [12]. However, the negative magnon frequencies imply that the optimized magnetic ground state may not be fully consistent with the magnetic interactions of Table III. A full classical optimization of magnetic structure again leads to a zigzag ground state, in which spins show significant out-of-plane tilting. Spectra obtained with this structure is shown in Fig. 7(c), which clearly is free of negative frequencies and show a 2-meV Goldstone gap. This gapped spectral feature is consistent with the previous experimental finding [12].

We now will briefly compare the properties of these two materials. Structurally, the crucial difference is the stacking of the Co honeycomb layers. For $Na_2Co_2TeO_6$, the layers are staggered, while for $Na_3Co_2SbO_6$, these layers are exactly on the top of each other. However, the estimated interlayer magnetic interactions in our calculations are found to be negligibly small ruling out any possibility of coupling between the honeycomb layers of Co in both these materials. The Co-Co distance in these two materials is very similar and comparatively larger deviation of Co-O-O angle from 90° between edge shared octahedra is found in $Na_3Co_2SbO_6$ ($\sim 93.5°$) when compared to the $Na_2Co_2TeO_6$ (92°) [14] as discussed earlier. This small difference does not seem to substantially affect the nearest-neighbor magnetic interactions. So while the 1NN interactions have similar strengths in both the materials (after averaging of two type of bonds in $Na_3Co_2SbO_6$), the smaller 3NN magnetic interactions in $Na_3Co_2SbO_6$ can be the reason behind its lower T_N (~ 7 K) than $Na_2Co_2TeO_6$ (T_N $\sim$

18 K). Also, the smaller off-diagonal η_3/η_3' in $Na_3Co_2SbO_6$ can be seen as a manifestation of the lower trigonal CF in $Na_3Co_2SbO_6$ as been explained in Liu *et al.* [13]. Thus, the smaller "undesirable" off-diagonal and 3NN terms make $Na_3Co_2SbO_6$ a more suitable candidate than $Na_2Co_2TeO_6$ in the quest of spin-liquid behavior.

In a recent study by Das *et al.* [51] on cobalt-based Kitaev materials, the authors commented, en passant, on the magnetic interactions in $Na_3Co_2SbO_6$. They found 1NN ferromagnetic Heisenberg and off-diagonal, antiferromagnetic 1NN Kitaev and 3NN Heisenberg couplings, all are of equal strength for this compound, differing from our results. It is important to verify that the combination of their magnetic interactions stabilizes the zigzag ground state, from following two considerations. First, the consensus seems to be that the zigzag ground state in these materials is a result of a combination of ferromagnetic K_1 and antiferromagtic J_1 and J_3 [10,13]. Second, though with 1NN antiferromagnetic Kitaev coupling where the nature of Heisenberg term is of lesser consequence, one may also realize a zigzag ground state. However, in this case the role of longer-range Heisenberg interaction requires further clarification [10,13].

V. SUMMARY AND REMARKS

In this paper, we investigated the structural and magnetic properties of $Na_2Co_2TeO_6$ and $Na_3Co_2SbO_6$. Using a cluster expansion model, we find a particular pattern of hexagonal lattice formation by Na vacancies in $Na_2Co_2TeO_6$. Using a multiband Hubbard model and the second-order perturbation theory valid in the large U regime, we have estimated the magnetic interactions in these material and showed that a zigzag magnetic order can only be stabilized when Kitaev term is either comparable to or larger than the first-neighbor Heisenberg term. However, we find the third-neighbor Heisenberg interaction to be the dominant magnetic interactions in both these compounds. In addition, we have also presented a phase diagram for $Na_2Co_2TeO_6$ by varying U and λ, a majority portion of which is shared by different zigzag magnetic ground state. Based on the spin Hamiltonian, we have calculated spin-wave spectra and showed that our findings are in qualitative agreement with the recent neutron-scattering experiments. A comparison between these two materials establish the fact that $Na_3Co_2SbO_6$ is might be a better candidate than $Na_2Co_2TeO_6$ in the quest for Kitaev materials due to smaller off-diagonal and 3NN magnetic interactions in the former.

The trigonal CF present in these materials is believed to be the main hurdle for realization of a quantum spin liquid phase and has been recently suggested as an experimentally tuneable parameter [13]. Previously, this type of tuning has been achieved experimentally by means of strain in CoO [52] and would be an interesting future direction of research at both theoretical and experimental fronts. For another interesting aspect from an experimental perspective, it will be worth investigating whether magnetic field can induce a quantum spin liquid phase in these cobalt-based compounds, alluding to another Kitaev candidate material α-$RuCl_3$ [53].

ACKNOWLEDGMENTS

We are grateful for stimulating discussions with Yuan Li. We acknowledge the financial support from the National Natural Science Foundation of China (Grants No. 11725415 and No. 11934001), the National Key R&D Program of China (Grants No. 2018YFA0305601 and No. 2021YFA1400100), and the Strategic Priority Research Program of Chinese Academy of Sciences (Grant No. XDB28000000).

APPENDIX: HOPPING AMPLITUDES

Hopping amplitudes between Co-d orbitals via X, Y and Z bonds

TABLE IV. 1NN and 3NN hopping amplitudes in $Na_2Co_2TeO_6$ estimated from Wannier interpolation of the *ab initio* band structure.

	1NN			3NN		
Hopping	X	Y	Z	X	Y	Z
$d_{z^2} \rightarrow d_{z^2}$	−0.0307	−0.0307	−0.0709	0.0806	0.0806	−0.0335
$d_{zx} \rightarrow d_{zx}$	0.0364	−0.1699	0.0364	0.0047	−0.0327	0.0047
$d_{yz} \rightarrow d_{yz}$	−0.1699	0.0364	0.0364	−0.0327	0.0047	0.0047
$d_{x^2-y^2} \rightarrow d_{x^2-y^2}$	−0.0575	−0.0575	0.0046	0.0046	0.0046	0.1187
$d_{xy} \rightarrow d_{xy}$	0.0364	0.0364	−0.1699	0.0047	0.0047	−0.0327
$d_{z^2} \leftrightarrow d_{zx}$	−0.0184	0.0638	0.0071	0.0082	0.0080	−0.0010
$d_{z^2} \leftrightarrow d_{yz}$	0.0638	−0.0184	0.0071	0.0085	0.0073	−0.0010
$d_{z^2} \leftrightarrow d_{x^2-y^2}$	0.0232	−0.0232	0.0000	0.0659	−0.0659	0.0000
$d_{z^2} \leftrightarrow d_{xy}$	−0.0114	−0.0114	0.1275	0.0072	0.0063	0.0161
$d_{zx} \leftrightarrow d_{yz}$	0.0467	0.0467	−0.0457	−0.0007	−0.0007	−0.0077
$d_{zx} \leftrightarrow d_{x^2-y^2}$	−0.0030	0.1104	−0.0176	0.0030	0.0146	0.0089
$d_{zx} \leftrightarrow d_{xy}$	0.0457	−0.0467	−0.0467	0.0077	0.0007	0.0006
$d_{yz} \leftrightarrow d_{x^2-y^2}$	−0.1098	0.0030	0.0176	−0.0139	−0.0036	−0.0089
$d_{yz} \leftrightarrow d_{xy}$	−0.0479	0.0457	−0.0467	0.0006	0.0077	0.0006
$d_{x^2-y^2} \leftrightarrow d_{xy}$	−0.0147	0.0146	0.0000	0.0053	−0.0048	0.0000

TABLE V. 1NN and 3NN hopping amplitudes in $Na_3Co_2SbO_6$ estimated from Wannier interpolation of the *ab initio* band structure.

	1NN			3NN		
Hopping	X	Y	Z	X	Y	Z
$d_{z^2} \rightarrow d_{z^2}$	0.0001	−0.0096	−0.0590	0.0060	0.0011	0.0244
$d_{zx} \rightarrow d_{zx}$	−0.1478	0.0390	0.0352	0.0049	0.0073	−0.0010
$d_{yz} \rightarrow d_{yz}$	0.0483	−0.1449	0.0272	0.0055	0.0047	−0.0071
$d_{x^2-y^2} \rightarrow d_{x^2-y^2}$	−0.0624	−0.0463	0.0060	0.0060	0.0206	0.0018
$d_{xy} \rightarrow d_{xy}$	0.0365	0.0365	−0.1312	0.0009	−0.0103	0.0029
$d_{z^2} \leftrightarrow d_{zx}$	−0.0482	0.0074	−0.0219	−0.0124	0.0176	−0.0159
$d_{z^2} \leftrightarrow d_{yz}$	−0.0021	0.0616	0.0220	−0.0158	0.0089	0.0096
$d_{z^2} \leftrightarrow d_{x^2-y^2}$	−0.0167	0.0270	−0.0223	0.0175	−0.0150	0.0016
$d_{z^2} \leftrightarrow d_{xy}$	0.0142	0.0059	−0.1213	−0.0018	0.0016	−0.0167
$d_{zx} \leftrightarrow d_{yz}$	−0.0106	−0.0336	0.0234	0.0059	−0.0019	0.0147
$d_{zx} \leftrightarrow d_{x^2-y^2}$	−0.1229	0.0032	0.0057	−0.0167	−0.0061	0.0134
$d_{zx} \leftrightarrow d_{xy}$	−0.0094	0.0239	−0.0497	0.0030	0.0042	−0.0094
$d_{yz} \leftrightarrow d_{x^2-y^2}$	0.0079	−0.1114	0.0205	−0.0154	−0.0171	0.0134
$d_{yz} \leftrightarrow d_{xy}$	−0.0221	0.0359	0.0529	−0.0423	−0.0026	−0.0060
$d_{x^2-y^2} \leftrightarrow d_{xy}$	0.0066	0.0189	−0.0246	−0.0278	0.0229	0.0013

[1] L. Balents, Nature (London) **464**, 199 (2010).
[2] P. Anderson, Mater. Res. Bull. **8**, 153 (1973).
[3] A. Kitaev, Ann. Phys. **321**, 2 (2006).
[4] P. W. Anderson, Science **235**, 1196 (1987).
[5] M. R. Norman, Rev. Mod. Phys. **88**, 041002 (2016).
[6] Y. Zhou, K. Kanoda, and T.-K. Ng, Rev. Mod. Phys. **89**, 025003 (2017).
[7] S. M. Winter, A. A. Tsirlin, M. Daghofer, J. van den Brink, Y. Singh, P. Gegenwart, and R. Valentí, J. Phys.: Condens. Matter **29**, 493002 (2017).
[8] H. Takagi, T. Takayama, G. Jackeli, G. Khaliullin, and S. E. Nagler, Nat. Rev. Phys. **1**, 264 (2019).
[9] G. Jackeli and G. Khaliullin, Phys. Rev. Lett. **102**, 017205 (2009).
[10] H. Liu and G. Khaliullin, Phys. Rev. B **97**, 014407 (2018).
[11] R. Sano, Y. Kato, and Y. Motome, Phys. Rev. B **97**, 014408 (2018).
[12] M. Songvilay, J. Robert, S. Petit, J. A. Rodriguez-Rivera, W. D. Ratcliff, F. Damay, V. Balédent, M. Jiménez-Ruiz, P. Lejay, E. Pachoud, A. Hadj-Azzem, V. Simonet, and C. Stock, Phys. Rev. B **102**, 224429 (2020).
[13] H. Liu, J. c. v. Chaloupka, and G. Khaliullin, Phys. Rev. Lett. **125**, 047201 (2020).
[14] L. Viciu, Q. Huang, E. Morosan, H. Zandbergen, N. Greenbaum, T. McQueen, and R. Cava, J. Solid State Chem. **180**, 1060 (2007).
[15] W. Chen, X. Li, Z. Hu, Z. Hu, L. Yue, R. Sutarto, F. He, K. Iida, K. Kamazawa, W. Yu, X. Lin, and Y. Li, Phys. Rev. B **103**, L180404 (2021).
[16] K. W. Plumb, J. P. Clancy, L. J. Sandilands, V. V. Shankar, Y. F. Hu, K. S. Burch, H.-Y. Kee, and Y.-J. Kim, Phys. Rev. B **90**, 041112(R) (2014).
[17] R. D. Johnson, S. C. Williams, A. A. Haghighirad, J. Singleton, V. Zapf, P. Manuel, I. I. Mazin, Y. Li, H. O. Jeschke, R. Valentí, and R. Coldea, Phys. Rev. B **92**, 235119 (2015).
[18] A. Banerjee, C. A. Bridges, J.-Q. Yan, A. A. Aczel, L. Li, M. B. Stone, G. E. Granroth, M. D. Lumsden, Y. Yiu, J. Knolle, S. Bhattacharjee, D. L. Kovrizhin, R. Moessner, D. A. Tennant, D. G. Mandrus, and S. E. Nagler, Nat. Mater. **15**, 733 (2016).
[19] J. c. v. Chaloupka, G. Jackeli, and G. Khaliullin, Phys. Rev. Lett. **105**, 027204 (2010).
[20] Y. Singh, S. Manni, J. Reuther, T. Berlijn, R. Thomale, W. Ku, S. Trebst, and P. Gegenwart, Phys. Rev. Lett. **108**, 127203 (2012).
[21] Y. Singh and P. Gegenwart, Phys. Rev. B **82**, 064412 (2010).
[22] S. K. Choi, R. Coldea, A. N. Kolmogorov, T. Lancaster, I. I. Mazin, S. J. Blundell, P. G. Radaelli, Y. Singh, P. Gegenwart, K. R. Choi, S.-W. Cheong, P. J. Baker, C. Stock, and J. Taylor, Phys. Rev. Lett. **108**, 127204 (2012).
[23] A. Biffin, R. D. Johnson, S. Choi, F. Freund, S. Manni, A. Bombardi, P. Manuel, P. Gegenwart, and R. Coldea, Phys. Rev. B **90**, 205116 (2014).
[24] A. Biffin, R. D. Johnson, I. Kimchi, R. Morris, A. Bombardi, J. G. Analytis, A. Vishwanath, and R. Coldea, Phys. Rev. Lett. **113**, 197201 (2014).
[25] J. G. Rau, Eric Kin-Ho Lee, and H.-Y. Kee, Phys. Rev. Lett. **112**, 077204 (2014).
[26] S. Nishimoto, V. M. Katukuri, V. Yushankhai, H. Stoll, U. K. Rößler, L. Hozoi, I. Rousochatzakis, and J. van den Brink, Nat. Commun. **7**, 10273 (2016).
[27] V. M. Katukuri, S. Nishimoto, V. Yushankhai, A. Stoyanova, H. Kandpal, S. Choi, R. Coldea, I. Rousochatzakis, L. Hozoi, and J. van den Brink, New J. Phys. **16**, 013056 (2014).
[28] Y. Sizyuk, C. Price, P. Wölfle, and N. B. Perkins, Phys. Rev. B **90**, 155126 (2014).
[29] J. C. V. Chaloupka and G. Khaliullin, Phys. Rev. B **92**, 024413 (2015).
[30] I. Kimchi, R. Coldea, and A. Vishwanath, Phys. Rev. B **91**, 245134 (2015).

[31] I. Kimchi and Y.-Z. You, Phys. Rev. B **84**, 180407(R) (2011).
[32] J. Reuther, R. Thomale, and S. Rachel, Phys. Rev. B **90**, 100405(R) (2014).
[33] Y. Yamaji, Y. Nomura, M. Kurita, R. Arita, and M. Imada, Phys. Rev. Lett. **113**, 107201 (2014).
[34] K. Foyevtsova, H. O. Jeschke, I. I. Mazin, D. I. Khomskii, and R. Valentí, Phys. Rev. B **88**, 035107 (2013).
[35] S. M. Winter, Y. Li, H. O. Jeschke, and R. Valentí, Phys. Rev. B **93**, 214431 (2016).
[36] W. Wang, Z.-Y. Dong, S.-L. Yu, and J.-X. Li, Phys. Rev. B **96**, 115103 (2017).
[37] Y. S. Hou, H. J. Xiang, and X. G. Gong, Phys. Rev. B **96**, 054410 (2017).
[38] G. Xiao, Z. Xia, W. Zhang, X. Yue, S. Huang, X. Zhang, F. Yang, Y. Song, M. Wei, H. Deng, and D. Jiang, Cryst. Growth Des. **19**, 2658 (2019).
[39] E. Lefrançois, M. Songvilay, J. Robert, G. Nataf, E. Jordan, L. Chaix, C. V. Colin, P. Lejay, A. Hadj-Azzem, R. Ballou, and V. Simonet, Phys. Rev. B **94**, 214416 (2016).
[40] A. K. Bera, S. M. Yusuf, A. Kumar, and C. Ritter, Phys. Rev. B **95**, 094424 (2017).
[41] J. P. Perdew, K. Burke, and M. Ernzerhof, Phys. Rev. Lett. **77**, 3865 (1996).
[42] G. Kresse and J. Furthmüller, Phys. Rev. B **54**, 11169 (1996).
[43] G. Kresse and D. Joubert, Phys. Rev. B **59**, 1758 (1999).
[44] P. E. Blöchl, Phys. Rev. B **50**, 17953 (1994).
[45] S. L. Dudarev, G. A. Botton, S. Y. Savrasov, C. J. Humphreys, and A. P. Sutton, Phys. Rev. B **57**, 1505 (1998).
[46] A. A. Mostofi, J. R. Yates, Y.-S. Lee, I. Souza, D. Vanderbilt, and N. Marzari, Comput. Phys. Commun. **178**, 685 (2008).
[47] M. Ångqvist, W. A. Muñoz, J. M. Rahm, E. Fransson, C. Durniak, P. Rozyczko, T. H. Rod, and P. Erhart, Adv. Theory Simul. **2**, 1900015 (2019).
[48] B. H. Kim, G. Khaliullin, and B. I. Min, Phys. Rev. B **89**, 081109(R) (2014).
[49] G. W. Pratt and R. Coelho, Phys. Rev. **116**, 281 (1959).
[50] S. Toth and B. Lake, J. Phys.: Condens. Matter **27**, 166002 (2015).
[51] S. Das, S. Voleti, T. Saha-Dasgupta, and A. Paramekanti, Phys. Rev. B **104**, 134425 (2021).
[52] S. I. Csiszar, M. W. Haverkort, Z. Hu, A. Tanaka, H. H. Hsieh, H.-J. Lin, C. T. Chen, T. Hibma, and L. H. Tjeng, Phys. Rev. Lett. **95**, 187205 (2005).
[53] S.-H. Baek, S.-H. Do, K.-Y. Choi, Y. S. Kwon, A. U. B. Wolter, S. Nishimoto, J. van den Brink, and B. Büchner, Phys. Rev. Lett. **119**, 037201 (2017).